Directionality of Interpersonal Neural Influence in fNIRS Hyperscanning: Validation of a Spectral Causality Approach in a Motor Task

Maha Shadaydeh[1], Vanessa Nöring[1], Marcel Franz[1], Tara Chand[2], Ilona Croy[1], and Joachim Denzler[1]

[1]FSU Jena
[2]O P Jindal Global (Institution of Eminence Deemed To Be University) Jindal Institute of Behavioural Sciences

February 20, 2025

Abstract

Hyperscanning approaches represent a shift from single- to two-person neuroscience, enabling a more profound understanding of the neural mechanisms underlying interpersonal synchronization. In this context, fNIRS has emerged as a valuable tool for measuring brain activity in a natural, unconstrained environment. While interpersonal synchrony using fNIRS hyperscanning has been well studied using statistical association analysis, establishing causal relationships that elucidate the direction of influence remains challenging. This study aimed to investigate the feasibility of testing the direction of influence in dyadic interactions. Since the ground truth of such direction is not available in a natural setting, we validated our approach in an experimental setup in which we controlled the direction of influence between two subjects by assigning them the roles of 'Model' and 'Imitator' of specified motor tasks. A total of 22 participants, hence 11 dyads, completed the task in a within-subject design. We adapted concepts from spectral causal-effect decomposition theories to formulate a new measure of the direction and intensity of influence. The results of this study demonstrate that the direction of influence in the fNIRs data of motor tasks can be detected with an Accuracy in the range of 69-88%. Furthermore, the proposed spectral causality measure was shown to significantly reduce spurious causal relationships due to the confounding effects of physiological processes and measurement artifacts compared to time-domain causal analysis.

Graphical Abstract

Directionality of Interpersonal Neural Influence in fNIRS Hyperscanning: Validation of a Spectral Causality Approach in a Motor Task

Maha Shadaydeh, Vanessa Noering, Marcel Franz, Tara Chand, Ilona Croy, Joachim Denzler

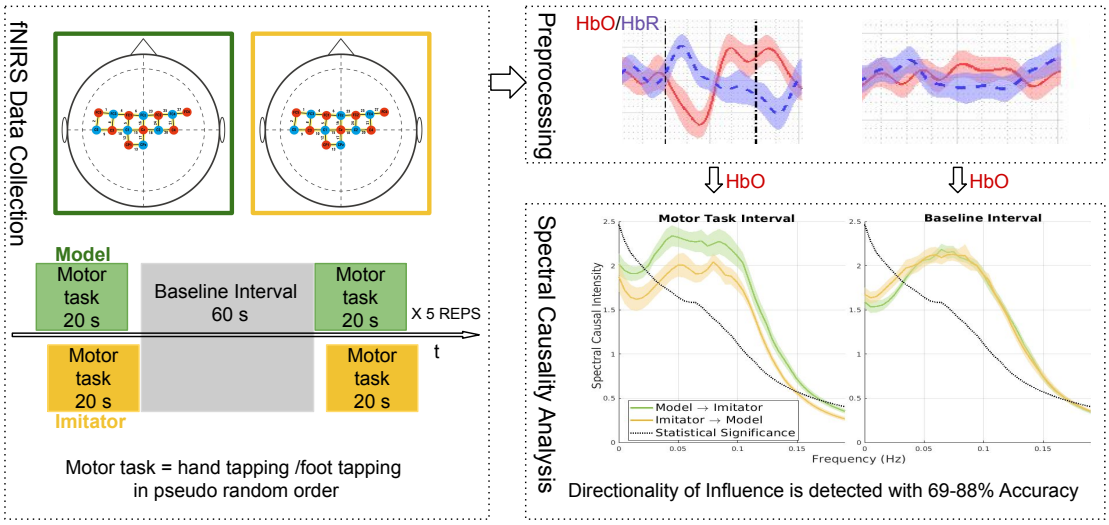

Highlights

Directionality of Interpersonal Neural Influence in fNIRS Hyperscanning: Validation of a Spectral Causality Approach in a Motor Task

Maha Shadaydeh, Vanessa Noering, Marcel Franz, Tara Chand, Ilona Croy, Joachim Denzler

- Causality analysis can reveal the direction of influence in fNIRS hyperscanning
- Experimental setup with a controlled direction of influence in motor imitation tasks
- Time and spectral group causality methods are investigated for directionality testing
- Spectral causality measure showed $69-88\%$ Accuracy in directionality detection
- Spectral causality analysis is more robust to measurement and physiological noises

Directionality of Interpersonal Neural Influence in fNIRS Hyperscanning: Validation of a Spectral Causality Approach in a Motor Task

Maha Shadaydeh[a,*], Vanessa Noering[b,c], Marcel Franz[b], Tara Chand[d], Ilona Croy[b,c], Joachim Denzler[a]

[a] *Department of Mathematics and Computer Science, Friedrich-Schiller-University of Jena, Ernst-Abbe Platz 2, Jena, 07743, Germany*
[b] *Department of Clinical Psychology, Institute of Psychology, Friedrich-Schiller-University of Jena, Am Steiger 3, Jena, 07743, Germany*
[c] *German Center for Mental Health, side Halle-Jena Magdeburg, Germany*
[d] *Jindal Institute of Behavioural Sciences, O. P. Jindal Global University, Sonipat, Haryana, India*

Abstract

Hyperscanning approaches represent a shift from single- to two-person neuroscience, enabling a more profound understanding of the neural mechanisms underlying interpersonal synchronization. In this context, fNIRS has emerged as a valuable tool for measuring brain activity in a natural, unconstrained environment. While interpersonal synchrony using fNIRS hyperscanning has been well studied using statistical association analysis, establishing causal relationships that elucidate the direction of influence remains challenging. This study aimed to investigate the feasibility of testing the direction of influence in dyadic interactions. Since the ground truth of such direction is not available in a natural setting, we validated our approach in an experimental setup in which we controlled the direction of influence between two subjects by assigning them the roles of 'Model' and 'Imitator' of specified motor tasks. A total of 22 participants, hence 11 dyads, completed the task in a within-subject design. We adapted concepts from spectral causal-effect decomposition theories to formulate a new measure of the direction and intensity of influence. The results of this study demonstrate that the direction of influence in the fNIRs data of motor tasks can be detected with an Accu-

*Corresponding author: maha.shadaydeh@uni-jena.de

racy in the range of $69 - 88\%$. Furthermore, the proposed spectral causality measure was shown to significantly reduce spurious causal relationships due to the confounding effects of physiological processes and measurement artifacts compared to time-domain causal analysis.

Keywords: fNIRS, hyperscanning, interpersonal synchronisation, social interaction; imaging; spectral causality, mutual information decomposition

1. Introduction

Hyperscanning involves the simultaneous recording of brain activity from two or more individuals to determine the temporal relation between both brains (synchronization). Hyperscanning approaches thereby mark a shift from single to two-person neuroscience, allowing a much deeper understanding of the neural mechanisms of interpersonal social interactions [1]. Such research revealed synchronized patterns of brain signals in interacting minds, especially in brain regions involved in social cognition, emotion, and motor control (for an overview, see [2]).

Different hyperscanning measurements such as EEG, fMRI, and functional near-infrared spectroscopy (fNIRS) have been used to investigate interpersonal synchronization during verbal, semi-verbal, and nonverbal interactions [3]. Compared to fMRI and EEG, fNIRS offers significant advantages for monitoring neural activity during natural, unconstrained, real-life interactions. Its high temporal resolution of oxygenation change and its motion tolerance make it particularly valuable for capturing dynamic neural activity in naturalistic settings [4].

While interpersonal synchrony using fNIRS hyperscanning has been well studied using statistical association analysis, e.g., temporal correlation [5] or wavelet coherence [6], establishing causal relationships that elucidate the direction of influence in hyperscanning remains challenging (for an overview, see [3]). This study aimed to go one step beyond the direction-blind statistical association and investigate the feasibility of testing the direction of influence in dyadic interactions using causal discovery methods.

Causal discovery in multivariate time series aims to elucidate the cause-and-effect relationships between variables that evolve over time. The most known classical method is Granger causality (GC) [7]. GC analyzes time series data to determine if one variable can predict future values of another target variable better than using past values of the target variable alone.

Recent research has increasingly focused on understanding the synergistic effects of groups of variables acting as a collective subsystem on other groups. This focus is particularly critical in complex systems characterized by intricate interdependencies, such as climate-ecosystem interactions and neural activity across distinct brain regions of the same subject [8]. Notable group causality methods are the Trace method [9], the 2GVecCI [10], Vanila-PC [11] and the Canonical-VAR (MC-VAR) [12]. While these methods operate in the time domain, Faes et al. [8] built on the spectral causality approach of Geweke [13] and proposed a framework based on mutual information rate (MIR) decomposition to assess the interactions among groups of processes, both within specific frequency bands of interest and in the time domain.

fNIRS data is often influenced by various sources of noise steaming from measurements and physiological processes, e.g., breathing, heart rate, Mayer waves, etc., [14]. In hyperscanning, these processes typically occur at similar frequency ranges in both participants and can confound the results, leading to spurious associations between participants when using time-domain statistical or causal analysis. Furthermore, the strength of coupling may vary across different frequency bands. To address these challenges, in our study, we adapted the framework of Faes et al., [8] to our problem and then proposed a new measure for the direction and intensity of causal effect relationships in fNIRS data. Since the ground truth of the direction of interpersonal influence is not available in a natural setting, we validated our approach in an experimental setup where we controlled the direction of influence between two subjects. We compared the results of different state-of-the-art group causality methods to the proposed spectral domain causal-effect measure and showed the feasibility of detecting the correct cause-effect direction in fNIRS time series data. To our knowledge, this paper is the first to provide a comprehensive analysis pipeline for identifying the direction of influence in fNIRS data.

2. Materials and Methods

2.1. Participants

A total of 11 dyads, 22 participants, were recruited from the student population, with a mean age of 23.15 and standard deviation of 2.58. The sample was 21 females and one male. Inclusion criteria required participants to be at least 18 years old and report to be neurologically healthy. Participants received research participation credits as compensation. The study

was conducted following the Declaration of Helsinki and approved by the ethics review board of the Faculty of Social and Behavioral Sciences of the University of Jena (FSV 22/063).

2.2. Experimental Design

Participants were invited in dyads to perform a dyadic movement imitation task. In the beginning, each person was assigned to either the role of Model or Imitator. Both participants were seated opposite each other, so the Model faced a screen behind the Imitator, invisible to the Imitator. We presented two 20-second videos on the screen, one showing hand-tapping and the other foot-tapping. For hand tapping, the video showed a person's hand with each finger (excluding the thumb) sequentially tapping on a surface at a rate of approximately 1.5 Hz. For the foot-tapping task, the video showed a barefoot tapping on the floor at the same rate. The Model's task was to watch the screen and copy the movement with their right hand or foot. The Imitator's task was to imitate the movement of the Model.

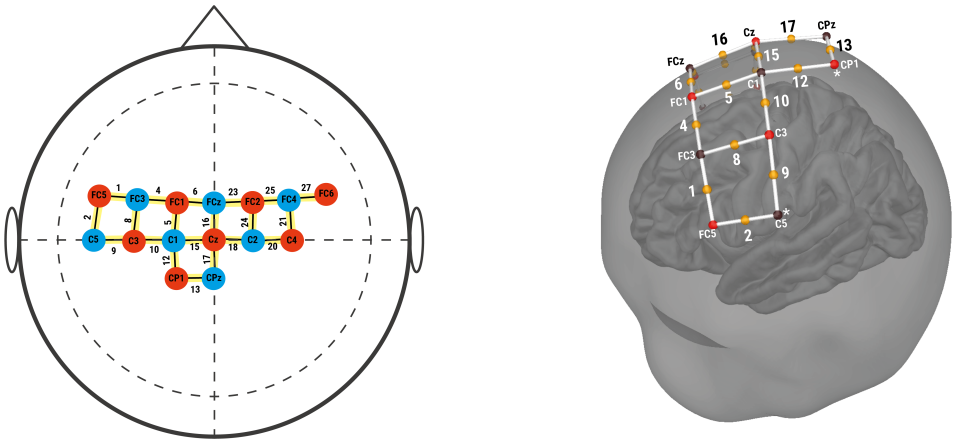

Figure 1: The optodes layout used for fNIRS measurements (2D and 3D views). The brain motor regions are M1 (Channels 12, 13, and 17), PMC (Channels 4, 5, 6, 8, and 16), and PMC/M1 (Channels 10 and 15).

A fixation cross was displayed for 60 seconds before each video, serving as a baseline during which participants were asked not to move. Videos were presented in a pseudo-randomized order five times each, resulting in ten trials per Model-Imitator constellation. After a short break, the Model

and Imitator switched roles and repeated the experiment with a different stimulus order. The experiment and the video presentation were programmed and controlled using Presentation software (Version 23.0, Neurobehavioral Systems, Inc., Berkley, CA).

2.3. fNIRS Data Acquisition

Each participant's cortical hemodynamic activity was recorded using a continuous wave fNIRS system (NIRSport2, NIRx, Germany) with a sampling rate of 10.17 Hz and 16 optodes per participant (eight emitters $\times$ eight detectors). Based on a finger- and foot-tapping study by Cockx et al. [15], the optodes were placed to cover the left and right primary motor cortex (M1) and premotor cortex (PMC) (Figure 1) with a distance of 3 cm to allow measurement of cerebral blood oxygenation at 2 to 3 cm depth. Additionally, eight short-distance channels were placed at each emitter position for later offline short-channel correction of non-neuronal signals from long-channel data.

2.4. fNIRS Data Preprocessing

The preprocessing of the fNIRS time series involved the following three steps, which were performed using the *fNIRSFilterPipeline* function of the Homer2 toolbox [16].

- Bandpass Filtering: A fifth-order Butterworth bandpass filter was applied with a low cutoff frequency of 0.02 Hz and a high cutoff frequency of 0.15 Hz. The phase of the used filter is almost linear in the passband, i.e., all signal components undergo a similar delay, and thus, no influence on causal analysis is expected due to this filtering process. This filtering step removes physiological noise, such as respiratory fluctuations ($\approx$ 0.25 Hz), cardiac oscillations ($\approx$ 1 Hz) [3], and slow drifts in the baseline signal, while preserving neural activity in the typical frequency range of interest ($\approx$ 0.029 Hz, depending on the stimulus presentation rate [3]).

- Hemoglobin Concentration Estimation: Changes in oxy/deoxygenated hemoglobin (HbO/HbR) concentrations were estimated using the modified Beer-Lambert law [17].

- Normalization: The preprocessed HbO and HbR time series were normalized to have zero mean and unit standard deviation.

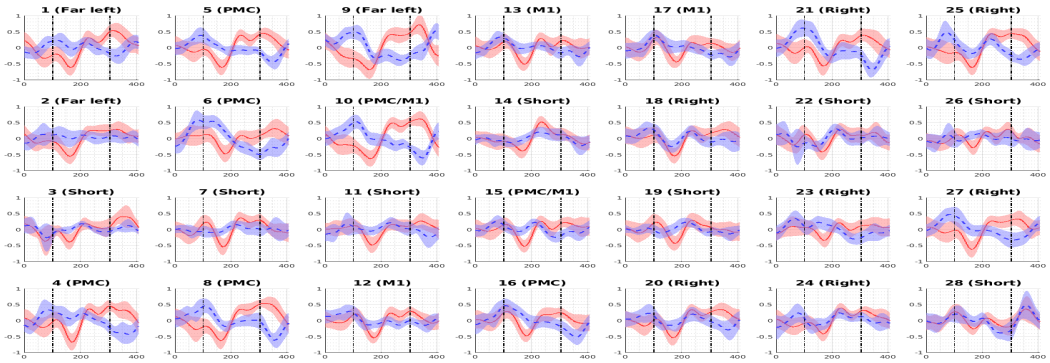

(a) Hand-Tapping

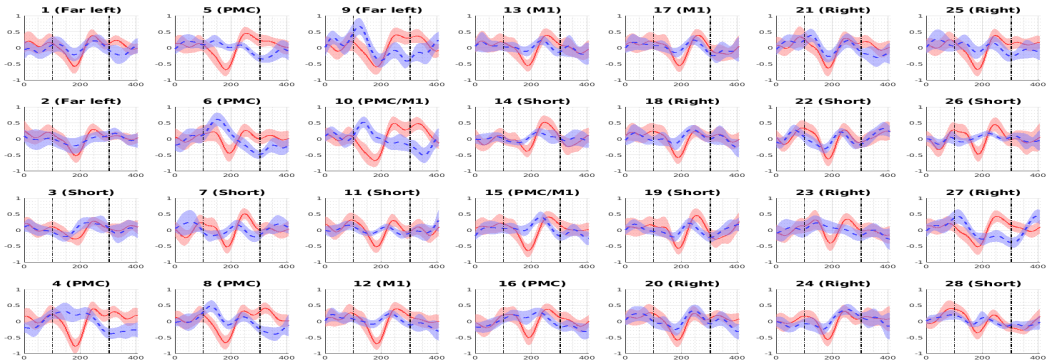

(b) Foot-Tapping

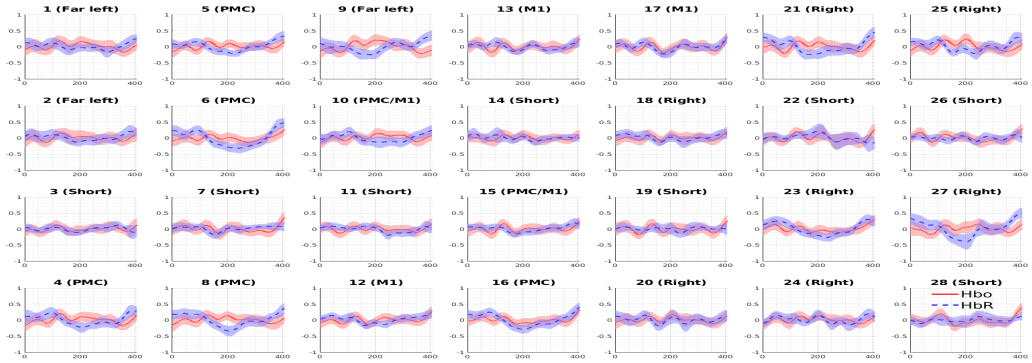

(c) Baseline

Figure 2: The average and 50% confidence interval of the normalized oxy-/de-oxygenated hemoglobin time series (HbO/HbR) in red/blue color. The time series are averaged for each channel over all dyads and task repetitions (total of 80 intervals) for (a) hand tapping, (b) foot tapping, and (c) baseline tasks. Each subplot spans a 40-second interval ($\approx$ 407 samples). The start and end of the motor task in motor task intervals are marked in vertical lines. For baseline intervals, we show the 40 seconds (407 samples) starting 20 seconds after the end of the motor task.

Data quality was assessed in the time domain using the *qualityAssessment* function within the Homer2 toolbox [16]. A supplementary wavelet-based visual quality control procedure [6] was implemented before the filtering process. Figure 5 in 6 shows examples of good and bad quality HbO signals. Eight of the eleven dyads exhibited good data quality and were included in the subsequent analysis.

Figure 2 illustrates the preprocessed signals for hand tapping, foot tapping, and baseline intervals. We can see an apparent increase in HbO signal during motor tasks (Figure 2 (a) and (b)) compared to the baseline condition (Figure 2 (c)) in the brain motor regions: M1 (Channels 12, 13, and 17), PMC (Channels 4, 5, 6, 8, and 16), and PMC/M1 (Channels 10 and 15). Residual periodic fluctuations, likely attributed to Mayer waves, are observable at ≈ 0.1 Hz ($\approx$ two waves in 20 seconds). Some short-distant channels, such as channels 7 and 14, displayed motor task-related activations. Thus, employing these channels for noise reduction in the fNIRS time series could potentially lead to the inadvertent removal of genuine neural activity. Since our proposed causal intensity measure, detailed in the following section, relies on the difference in cross-spectral densities of the information flow between the two participants, we excluded short-distance channels from subsequent analyses.

2.5. The Directionality of Neural Influence: A Spectral Causality Approach

To identify the direction of influence between the two participants (Model and Imitator) within each dyad, we adapted the Spectral Decomposition of Mutual Information Rate framework (MIR) of [13, 8], hereafter referred to as Spectr-MIR. In the following, we first provide a brief overview of the Spectr-MIR method as adapted to our problem and subsequently propose our definition of the measure quantifying both the intensity and direction of the causal effect between the Model and the Imitator along with the used statistical significance test.

2.5.1. Spectr-MIR Method

Let $X(t_n) \in \mathbb{R}^{L\times 2N}$ be $L \times 2N$ matrix representing N time series of length L of a specific brain region for both the Model (M) and Imitator (I), respectively, where $t_n = n\Delta t$ is the time index in iteration n and $\Delta t = 1/f_s$ with f_s the sampling frequency. The matrix $X(t_n)$ can be represented as the concatenation of the HbO channels of the Model X_M and Imitator X_I as $X(t_n) = [X_M(t_n) \quad X_I(t_n)]$. The information shared by the two random

processes $X_M(t_n)$ and $X_I(t_n)$ per unit of time is defined as the mutual information rate (MIR) as follows [18]

$$\mathrm{MIR}_{X_M;X_I} = \lim_{k\to\infty} \frac{1}{k}\mathrm{MI}\left(X_M(t_{n-k:n-1}); X_I(t_{n-k:n-1})\right), \tag{1}$$

where $\mathrm{MI}(X_1, X_2)$ denotes the mutual information (MI) shared by the two variables X_1 and X_2 and defined as

$$\mathrm{MI}(X_1; X_2) = \mathbb{E}\left[\log \frac{p(x_1, x_2)}{p(x_2)p(x_1)}\right]. \tag{2}$$

where $p(.,.)$ and $p(.)$ denote joint and marginal probabilities, and $\mathbb{E}$ is the statistical expectation operator. Using the relation between transfer entropy and mutual information, it is possible to decompose the MIR into three components, that is [8, 18]

$$\mathrm{MIR}_{X_M;X_I} = T_{X_M\to X_I} + T_{X_I\to X_M} + \mathrm{MIR}_{X_M.X_I}. \tag{3}$$

$\mathrm{MIR}_{X_M.X_I}$ represents the instantaneous information shared between X_M and X_I and $T_{X_i\to X_j}$ is the entropy transfer from X_i to X_j.

Following the methodology of [18, 8], we utilize a state-space modeling approach to compute all necessary MIR terms. Accordingly, we present the process $X(t_n)$ as a state space model, i.e.,

$$\begin{aligned} S(t_{n+1}) &= \mathbf{A}S(t_n) + \mathbf{K}W(t_n), \\ X(t_n) &= \mathbf{C}S(t_n) + W(t_n). \end{aligned} \tag{4}$$

$S(t_n)$ is the $2N \times p$ state vector of the model, where p is the model order; $\mathbf{A}, \mathbf{C}$ and $\mathbf{K}$ are the state-space model matrices, and $W(t_n)$ is a white Gaussian innovation noise vector of zero mean and Covariance matrix $\mathbf{\Sigma}_W = \mathbb{E}[W_n W_n^T]$. Similar to $X(t_n)$, $W(t_n)$ also can be written as $W(t_n) = [W_M(t_n) \quad W_I(t_n)]$.

Taking the Fourier Transform (FT) of the state Equation 4 yields

$$S(\omega) = \mathbf{A}S(\omega)e^{-\mathbf{j}\omega} + \mathbf{K}W(\omega)e^{-\mathbf{j}\omega}, \tag{5}$$

where $S(\omega)$ and $W(\omega)$ are respectively the Fourier transforms of $S(t_n)$ and $W(t_n)$ and ω is the normalized angular frequency. From Equation 5 we can derive the power spectral density of $X(t_n)$ as $X(\omega) = \mathbf{H}(\omega)W(\omega)$, where

$$\mathbf{H}(\omega) = \left(\mathbf{I}_{2N\times p} + \mathbf{C}[\mathbf{I}_{2N\times p} - \mathbf{A}e^{-\mathbf{j}\omega}]^{-1}\mathbf{K}e^{-\mathbf{j}\omega}\right), \tag{6}$$

with $\mathbf{I}$ being the identity matrix. $\mathbf{H}(\omega)$ represents the transfer function relating the FT of the innovation process $W(t_n)$ to the FT of the process $X(t_n)$ and can be used together with the innovation covariance matrix to derive the power spectral density (PSD) matrix of the process $X(t_n)$ using spectral factorization.

$$\mathbf{S}_X(\omega) = \mathbf{H}(\omega)\mathbf{\Sigma}_W\mathbf{H}^*(\omega). \tag{7}$$

The matrix $\mathbf{S}_X(\omega)$ can be then factorized to get the power spectral densities of X_M and X_I, $\mathbf{S}_{X_M}(\omega)$ and $\mathbf{S}_{X_I}(\omega)$ and the cross-spectral densities between X_M and X_I, $\mathbf{S}_{X_M X_I}(\omega)$ and $\mathbf{S}_{X_I X_M}(\omega)$. A logarithmic spectral measure of the interdependence between X_M and X_I is defined by [13].

$$f_{X_I;X_M}(\omega) = \log \frac{|\mathbf{S}_{X_I}(\omega)||\mathbf{S}_{X_M}(\omega)|}{|\mathbf{S}_X(\omega)|}, \tag{8}$$

where $f_{X_I;X_M}(\omega)$ is a measure of the total spectral coupling between X_I and X_M, which, in analogy to the time domain decomposition, can be factorized into three components.

$$f_{X_I;X_M}(\omega) = f_{X_I \to X_M}(\omega) + f_{X_M \to X_I}(\omega) + f_{X_I.X_M}(\omega), \tag{9}$$

where $f_{X_{(1)} \to X_{(2)}}(\omega)$ is a measure of the density of information transferred from process $X_{(1)}$ to process $X_{(2)}$, and $f_{X_I.X_M}(\omega)$ is the information shared between the two processes at angular frequency ω. These measures are defined as

$$f_{X_I.X_M}(\omega) = \log \frac{|\mathbf{H}_M(\omega)\mathbf{\Sigma}_{W_M}\mathbf{H}_M^*(\omega)||\mathbf{H}_I(\omega)\mathbf{\Sigma}_{W_I}\mathbf{H}_I^*(\omega)|}{|\mathbf{S}_X(\omega)|}, \tag{10}$$

$$f_{X_M \to X_I}(\omega) = \log \frac{|\mathbf{S}_{X_I}(\omega)|}{|\mathbf{H}_M(\omega)\mathbf{\Sigma}_{W_M}\mathbf{H}_M^*(\omega)|}, \tag{11}$$

$$f_{X_I \to X_M}(\omega) = \log \frac{|\mathbf{S}_{X_M}(\omega)|}{|\mathbf{H}_I(\omega)\mathbf{\Sigma}_{W_I}\mathbf{H}_I^*(\omega)|}. \tag{12}$$

Here, $\mathbf{H}_{(\cdot)}(\omega)$ describes the transfer from $\mathbf{W}_{(\cdot)}$ to $X_{(\cdot)}$ in the frequency domain and $\mathbf{\Sigma}_{W_{(\cdot)}} = \mathbb{E}[W_{(\cdot),n}W_{(\cdot),n}^T]$.

In our study, the full state space model, as defined in Equation 4, represents only the channels of the two regions of interest in the Model and Imitator and not the channels of all regions in both participants. We justify our choice by arguing that we are only interested in the inter-dependencies

of a specific brain region in both Model and Imitator, regardless of the intra-dependency of other regions in the same person's brain. Moreover, focusing on a specific brain region at a time can benefit from better model fitting due to lower dimensionality since the intervals of the motor task are only of size 200 samples, which is insufficient to accurately fit a higher dimensionality model.

2.5.2. Spectral Causal Intensity Measure

Our objective was to measure the intensity and direction of the cause-effect relationship between a specific region in the brain of the Model and the same region of the Imitator. Model and Imitator are, in principle, two independent entities. In our settings, any bidirectional causality and/or detected cause-effect during baseline intervals presumably results from some unobserved factor influencing both participants, such as a physiological process occurring at the same frequency range, task repetition frequency, or common noise occurring during signal measurement and acting as a confounder. To eliminate, as much as possible, any causality due to confounders, we propose to measure the causal effect of the Model on the Imitator in the frequency domain at frequency ω as

$$C_{X_M,X_I}(\omega) = f_{X_M \to X_I}(\omega) - f_{X_I \to X_M}(\omega) \tag{13}$$

2.5.3. Statistical Significance of Spectr-MIR

To assess the statistical significance of the causal relationships identified, we use a frequency domain surrogate data method [19]. This approach preserves the amplitude spectrum of the original HbO time series while randomising the phase information, effectively breaking the temporal dependencies within the data. The following steps are applied to the HbO time series: 1. Compute the Fourier transform of the original HbO time series. 2. Replace the original phase of each Fourier coefficient with a random phase drawn from a uniform distribution between 0 and 2π. 3. Perform the inverse Fourier transform to produce a surrogate HbO time series. 4. Apply the same causal inference method described above to the generated surrogate HbO time series. This procedure is repeated several times to produce an ensemble of surrogate time series. The spectral causality value of the HbO time series data is considered significant at a specific frequency only if it exceeds the spectral causality of the surrogate data at this frequency.

2.6. The Directionality of Neural Influence: Time Domain Causal Analysis

2.6.1. Spectr-MIR

The time domain causal intensity and direction for the Spectr-MIR method can be obtained by the integration of $C_{X_M,X_I}(\omega)$ over a specific band of frequencies from ω_1 to ω_2

$$C_{X_M \to X_I} = \frac{1}{4\pi} \int_{\omega_1}^{\omega_2} C_{X_M,X_I}(\omega) \mathrm{d}\omega \tag{14}$$

We define the intensity of the causal effect as the absolute value of $C_{X_M \to X_I}$, and the direction of the causal effect based on the sign of $C_{X_M \to X_I}$. Specifically, for $C_{X_M,X_I} > 0$ the direction of influence is from model X_M to Imitator X_I. Otherwise, if $C_{X_M,X_I} < 0$ then the direction of influence is from Imitator X_I to Model X_M. For $C_{X_M,X_I} = 0$, we assume there is no causal effect between The Model X_M and Imitator X_I. This definition supports the elimination of spurious causal influence between the Model and the Imitator due to noise and physiological processes that the filtering step of preprocessing could not eliminate.

2.6.2. Baseline Time Domain Group Causality Methods

To assess the performance of the proposed time domain causal direction estimation using the Spectr-MIR method, we compare it with the following four state-of-the-art time domain group causality methods.

- Vanilla-PC Method [11]: A framework for inferring causal directions between groups of variables by applying a series of conditional independence tests.

- Trace method [9]: This method infers whether linear relations between two high-dimensional variables X and Y are due to a causal influence from X to Y or from Y to X.

- 2GVecCI [10]: A non-parametric approach for inferring the causal relationship between two vector-valued random variables from observational data based on a series of conditional independence tests.

- Canonical Granger Causality method (MC-VAR) [12]: This method combines ideas from canonical correlation and Granger causality analysis to yield a measure that reflects directed causality between two regions of interest using optimized linear combinations of signals from each region of interest to enable accurate causality measurements.

2.6.3. Evaluation Metrics

To validate the performance of time domain group causal analysis methods, we calculated the following metrics: Accuracy, false positive rate (FPR), true positive rate (TPR), and F-Score. TPR presents the ratio of intervals of a specific motor task of all dyads and task repetitions where the causality direction is correctly detected from Model to Imitator. Meanwhile, FPR is the ratio of intervals for a specific motor task of all dyads and task repetitions where the causality direction is falsely detected from the Imitator to the Model. Accuracy is the ratio of intervals where the causal link from the Model to the Imitator in motor tasks and the absence of causal link in the baseline intervals are correctly predicted. The F-score focuses more on the correctly detected links in motor task intervals. Formally, these metrics are defined as follows.

$$\text{Accuracy} = \frac{\text{TP+TN}}{\text{TP+FP + TN+FN}} \tag{15}$$

$$\text{FPR} = \frac{\text{FP}}{\text{FP + TN}} \tag{16}$$

$$\text{TPR} = \frac{\text{TP}}{\text{FP + TN}} \tag{17}$$

$$\text{F-score} = \frac{\text{TP}}{\text{TP} + 0.5(\text{FP + FN})} \tag{18}$$

Here, TP is the number of trials where the correct direction from Model to Imitator is detected; TN is the number of trials where no causal link from Model to Imitator or from Imitator to Model is correctly detected in baseline intervals. FP is the number of baseline intervals where a causal link is falsely detected; FN is the number of motor task intervals where no causal link is detected in either direction. Accuracy is our primary metric for evaluation, but other metrics help better understand the methods' overall performance.

3. Results

3.1. Spectral Causal Analysis Results

To evaluate the performance of the Spectr-MIR method in the frequency domain, we applied the method for each motor task and for each of the brain motor regions of interest, namely M1 (Channels 12, 13, and 17), PMC (Channels 4, 5, 6, 8, and 16), and PMC/M1 (Channels 10 and 15) separately.

As we noted a delay in the activation of HbO in response to the motor task, we chose to work with an interval length of 224 samples, which is equal to the samples of task interval ($20 seconds \times 10.17 Hz \approx 204$ samples) and a slight shift of 10 samples (one-second of data) before and after the start and end of the motor task respectively. The spectral causality components (Equation 9) are calculated for each interval and each dyad and then averaged over all dyads and the ten repetitions of the same motor task.

In all our experiments, we used the *oir_mir* function of the Matlab toolbox of Faes et al., [8] to calculate the different components of spectral causality with adaptation to our definition of the state-space model as detailed in Section 2.5.1. Experimental results for the spectral group causality analysis using the Spectr-MIR method and for different brain regions are shown in Figure 3. These results indicate that the average spectral causality from Model to Imitator is higher than from Imitator to Model in hand-tapping and foot-tapping in almost all brain regions of interest. However, in baseline intervals of all brain regions, we see almost equal spectral causality in both directions. The statistically significant spectral causality in both directions during baseline intervals can be attributed to the confounding effect of the task repetition frequency as well as the confounding effect of measurement and physiological processes. The causal intensity at a specific frequency can be measured as defined by Equation 13 or directly from the difference between the green and orange lines.

Region-wise, we can notice in Figure 3 a higher causal intensity from Model to Imitator in motor task intervals in M1 and PMC/M1 regions compared to PMC. The hand-tapping intervals have a higher average causal intensity in the PMC/M1 region, while the causal intensity due to the foot-tapping task is higher in the M1 region. This difference in causal intensity between regions could be because the PMC/M1 covers more lateral parts, M1 covers more central parts, and the hand region is better represented in the lateral areas than the foot region [20].

3.2. Time-Domain Causal Analysis Results

In this section, we compare the Accuracy of estimating the direction of influence using the time domain Spectr-MIR (Section 2.6.1) with the time-domain group causality baseline methods described in Section 2.6.2: Trace methods [9], Vanilla PC [11], MC-VAR [12] and 2GVecCI [10].

The time domain causal intensity and direction for the Spectr-MIR using the integral of Equation 14 is calculated to include only statistically signifi-

cant values in the frequency range 0.02-0.15 Hz. The statistical significance for each dyad was estimated using the frequency surrogate data method described in Section 2.5.3 averaged over 10 surrogates.

Results are shown in Figure 4 for the brain regions PMC, M1, and PMC/M1. As a performance measure, we show the Accuracy and the false positive rate (FPR) in Figure 4, while the True Positive Rate (TPR) and F-score are shown in Figure Figure 6 in section 6.

For the foot tapping task, the best result of Spectr-MIR is from the M1 region (Accuracy= 88%, FPR = 0), and the worst is from the PMC region (Accuracy= 69%, FPR=0.08). On the other hand, for the hand tapping task, the best results are from the PMC/M1 region (Accuracy= 82%, FPR = 0), and the worst is from the M1 regions (Accuracy= 63%, FPR = 0.02). These ROI-wise results are consistent with similar differences in causal intensity results in PMC/M1 and M1 regions, as discussed in Section 3.1. For baseline intervals, the absence of causality is best detected in the M1 region (Accuracy= 88%, FPR=0.06) and worst in the PMC/M1 region (Accuracy= 75%, FPR = 0.12).

On average, Accuracy is higher for the foot-tapping task than the hand-tapping task. The higher Accuracy for foot tapping is probably due to a longer delay in HbO activation between the Model and the Imitator. As noted earlier, Figure 2 shows that the reaction time is longer for the foot than for the hand. This longer delay made it easier for causality methods to detect who leads (the cause) and who follows (the effect).

In almost all brain regions of interest, Spectr-MIR has higher accuracy and lower FPR than all other methods, followed by the Vanilla-PC method. The MC-VAR and Trace methods suffer from high FPR. The low FPR of the proposed causal intensity measure, based on the subtraction of the Spectr-MIR spectral causality $f_{X_M \to X_I}(\omega)$ from $f_{X_I \to X_M}(\omega)$, allowed the removal of spurious causal effects that could be attributed to measurement artifact or physiological processes.

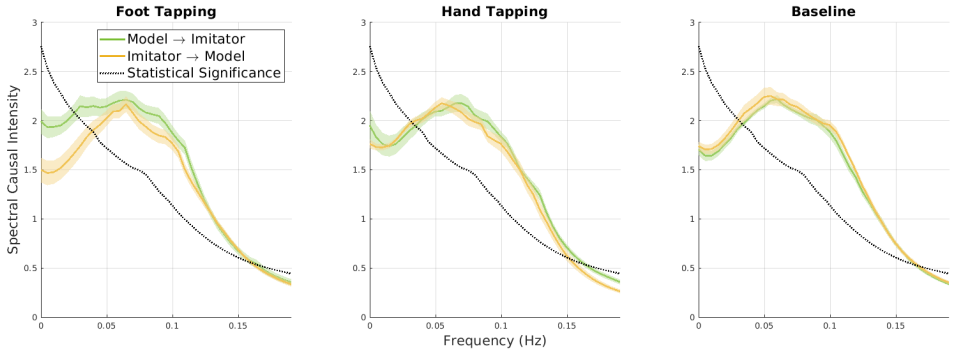

(a) PMC

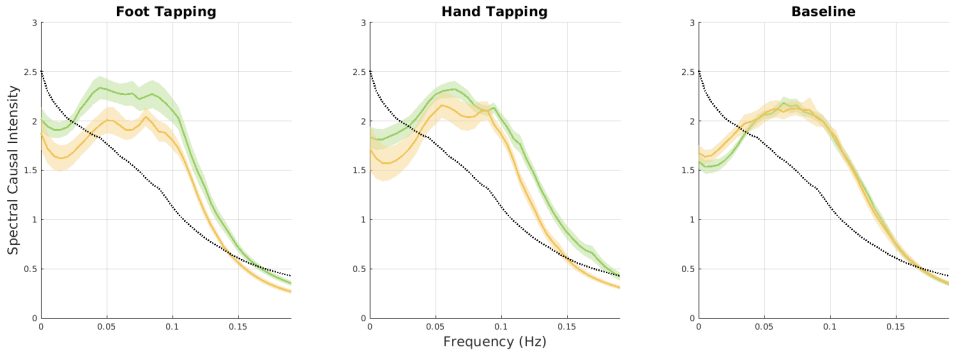

(b) M1

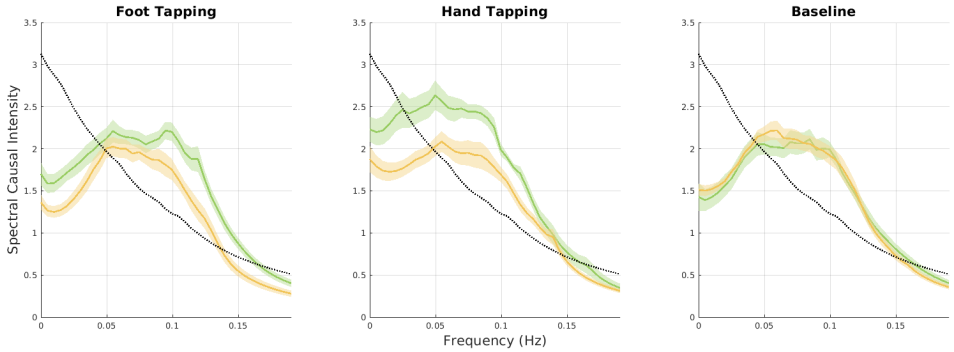

(c) PMC/M1

Figure 3: The average and 50% confidence interval of the spectral causality of the normalized HbO time series from Model to Imitator (green plots) and from Imitator to Model (orange plots). The average is calculated for each type of event of all dyads for regions: (a) Premotor cortex (PMC), (b) Primary motor cortex (M1), and (c) PMC/M1. The statistical significance is shown in the dotted black line, which is the average spectral causality of the frequency domain surrogate data. Only spectral causality values higher than this line are considered statistically significant.

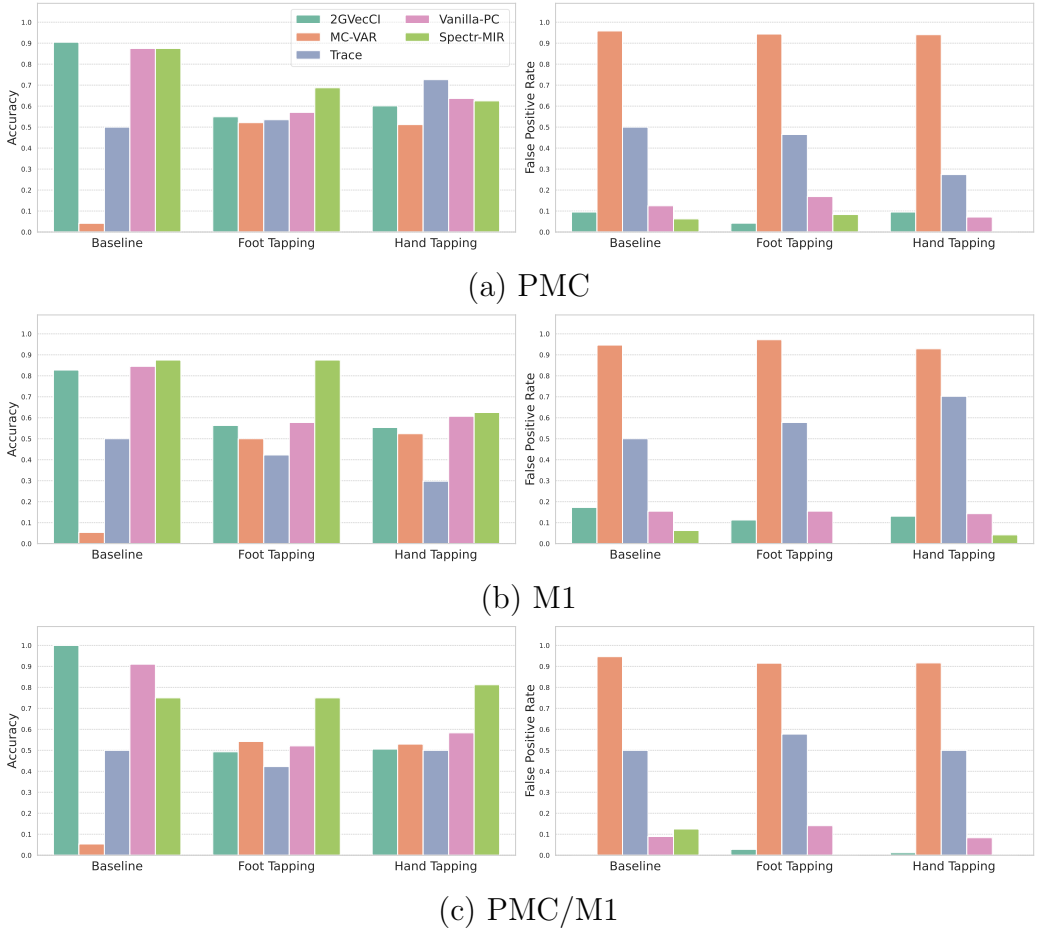

(a) PMC

(b) M1

(c) PMC/M1

Figure 4: Results of the time domain cause-effect analysis of the normalized HbO time series using the Spectr-MIR method in comparison with four baseline methods: Vanilla-PC [11], 2GVecCI [10], Trace [9], and MC-VAR [12]. The left column shows the Accuracy (higher is better) for the three different regions: (a) premotor cortex (PMC), (b) primary motor cortex (M1), and (c) PMC/M1. The right column shows the false positive rate (FPR) for the same methods and regions (lower is better).

3.3. Discussion

Both spectral and time domains causal analysis showed that causality can be accurately derived from fNIRs hyperscanning of motor tasks. Our causality measure achieved $69 - 88\%$ Accuracy in detecting the causal influence from Model to Imitator. Moreover, the proposed causality measure significantly reduced the false positive rate compared to time domain baseline causality methods (Figure 4). This reduction indicates that the proposed

measure enabled the removal of spurious causal effects that might result from task repetition, measurement, or physiological processes. The feasibility of detecting causality in fNIRS was not only significantly above chance but also significantly higher than the Accuracy of four other tested time domain methods. The average spectral cause-effect plots in Figure 3 showed a higher causality from the Model to Imitator than Imitator to Model for hand- and foot-tapping for all regions of interest. Our paradigm was not ambiguous in who leads and who follows in the interaction and was consistent with 10 very well-defined onset blocks of a standardized motor test typically evoking large responses. The motor imitation task deemed us a good testing paradigm, as it allows for valid control of causality - as only the Model saw the instruction, the Imitator's movement was dependent on the Model. The extracted HbO time series supported the validity of the task: The motor tasks led to an evident signal rise in the expected brain areas. We see evident activation of the averaged HbO time series during the motor tasks compared to baseline (Figure 2). The signal maximum occurred with a delay of about 10 seconds, in line with the temporal evolvement of the hemodynamic response function [21], and was faster for the hand than the foot. In the natural setting of fNIRS paradigms, such as cooperation tasks, data onset is less defined, and hence, we expect a worse signal-to-noise ratio for the detection of causal relations. The feasibility of our method for various natural settings needs further investigation.

4. Conclusion

This study aimed to test whether the direction of influence in dyadic interaction can be derived from fNIRs hyperscanning. To this end, we amended the frequency domain mutual information rate decomposition frameworks of Geweke [13] and Faes et al., [8] to fNIRS data of the motor imitation task. We then defined a measure for the direction and intensity of neural influence in frequency and time domains and compared the performance of this measure with four state-of-the-art time domain causal analysis methods. Our study showed that detecting the direction and intensity of neural influence is feasible based on fNIRs data. The usability of the proposed approach in a natural or uncontrolled setting might face new challenges that need further investigation. The varying magnitude and temporal delay in HbO activation in response to different tasks make it more challenging for the causal discovery methods to detect the correct cause-effect patterns in a natural setting

where several motor or non-motor tasks might occur simultaneously. We argue that using multimodal imaging or different sources of information is vital for causal discovery in fNIRS hyperscanning. Including emotional influence analysis using facial expressions in dyadic interaction [22], body-part-tracking, or verbal signal analysis as additional synchronization measures might support the validation of hyperscanning measurements-based causal discovery results.

5. Acknowledgment

This research is funded by the Federal Ministry of Education and Research (BMBF) project 01EW2105: "DZPG development funding – 'Jena location' – CIRC - (Mal)adaptive brain circuits of social interaction, FSU" as well as the German Research Foundation (DFG) individual research grant SH 1682/1-1.

6. Conflicts of Interest

The authors declare no conflicts of interest.

References

[1] A. Czeszumski, S. Eustergerling, A. Lang, D. Menrath, M. Gerstenberger, S. Schuberth, F. Schreiber, Z. Z. Rendon, P. König, Hyperscanning: A valid method to study neural inter-brain underpinnings of social interaction, Frontiers in Human Neuroscience 14 (2020). doi:10.3389/fnhum.2020.00039.

[2] S. De Felice, T. Chand, I. Croy, V. Engert, P. Goldstein, C. B. Holroyd, P. Kirsch, S. Krach, Y. Ma, D. Scheele, M. Schurz, S. R. Schweinberger, S. Hoehl, P. Vrticka, Relational neuroscience: Insights from hyperscanning research, Neuroscience Biobehavioral Reviews 169 (2025) 105979. doi:https://doi.org/10.1016/j.neubiorev.2024.105979.

[3] U. Hakim, S. D. Felice, P. Pinti, X. Zhang, J. A. Noah, Y. Ono, P. W. Burgess, A. Hamilton, J. HIRSCH, I. Tachtsidis, Quantification of inter-brain coupling: A review of current methods used in haemodynamic and electrophysiological hyperscanning studies, NeuroImage 280 (2023) 120354. doi:10.1016/j.neuroimage.2023.120354.

[4] P. Pinti, I. Tachtsidis, A. Hamilton, J. Hirsch, C. Aichelburg, S. Gilbert, P. W. Burgess, The present and future use of functional near-infrared spectroscopy (fnirs) for cognitive neuroscience, Annals of the New York Academy of Sciences 1464 (2020) 5–29. doi:https://doi.org/10.1111/nyas.13948.

[5] J. Han, H. Li, J. Cui, Q. Lan, L. Wang, Psychology-inspired interaction process analysis based on time series, in: 2022 26th International Conference on Pattern Recognition (ICPR), 2022, pp. 1004–1011. doi:10.1109/ICPR56361.2022.9956367.

[6] T. Nguyen, S. Hoehl, P. Vrtička, A guide to parent-child fnirs hyperscanning data processing and analysis, Sensors 21 (2021). URL: https://www.mdpi.com/1424-8220/21/12/4075. doi:10.3390/s21124075.

[7] C. W. J. Granger, Investigating causal relations by econometric models and cross-spectral methods, Econometrica 37 (1969) 424–438. URL: http://www.jstor.org/stable/1912791.

[8] L. Faes, G. Mijatovic, Y. Antonacci, R. Pernice, C. Barà, L. Sparacino, M. Sammartino, A. Porta, D. Marinazzo, S. Stramaglia, A new framework for the time- and frequency-domain assessment of high-order interactions in networks of random processes, IEEE Transactions on Signal Processing 70 (2022) 5766–5777. doi:10.1109/TSP.2022.3221892.

[9] J. Zscheischler, D. Janzing, K. Zhang, Testing whether linear equations are causal: A free probability theory approach, AUAI Press, Corvallis, OR, USA, 2011, pp. 839–847.

[10] J. Wahl, U. Ninad, J. Runge, Vector causal inference between two groups of variables, in: Proceedings of the AAAI Conference on Artificial Intelligence, volume 37, 2023, pp. 12305–12312.

[11] D. Janzing, P. O. Hoyer, B. Schölkopf, Telling cause from effect based on high-dimensional observations, arXiv preprint arXiv:0909.4386 (2009).

[12] S. Ashrafulla, J. P. Haldar, A. A. Joshi, R. M. Leahy, Canonical granger causality between regions of interest, NeuroImage 83 (2013) 189–199.

[13] J. Geweke, Measurement of linear dependence and feedback between multiple time series, Journal of the American Statistical Association 77 (1982) 304–313. doi:10.1080/01621459.1982.10477803.

[14] P. Pinti, F. Scholkmann, A. Hamilton, P. W. Burgess, I. Tachtsidis, Current status and issues regarding pre-processing of fnirs neuroimaging data: An investigation of diverse signal filtering methods within a general linear model framework, Frontiers in Human Neuroscience 12 (2019). URL: https://api.semanticscholar.org/CorpusID:57761210.

[15] H. Cockx, R. Oostenveld, M. Tabor, E. Savenco, A. van Setten, I. Cameron, R. van Wezel, fnirs is sensitive to leg activity in the primary motor cortex after systemic artifact correction, NeuroImage 269 (2023) 119880. URL: https://www.sciencedirect.com/science/article/pii/S1053811923000290. doi:https://doi.org/10.1016/j.neuroimage.2023.119880.

[16] T. Huppert, S. Diamond, M. Franceschini, D. Boas, Homer: a review of time-series analysis methods for near-infrared spectroscopy of the brain, Applied optics (2009). URL: https://dx.doi.org/10.1364/ao.48.00d280.

[17] D. T. Delpy, M. Cope, P. van der Zee, S. Arridge, S. Wray, J. Wyatt, Estimation of optical pathlength through tissue from direct time of flight measurement, Physics in Medicine Biology 33 (1988) 1433. doi:10.1088/0031-9155/33/12/008.

[18] T. E. Duncan, On the calculation of mutual information, SIAM Journal on Applied Mathematics 19 (1970) 215–220. doi:10.1137/0119020.

[19] J. Theiler, S. Eubank, A. Longtin, B. Galdrikian, J. Doyne Farmer, Testing for nonlinearity in time series: the method of surrogate data, Physica D: Nonlinear Phenomena 58 (1992) 77–94. doi:https://doi.org/10.1016/0167-2789(92)90102-S.

[20] L. V. Metman, J. S. Bellevich, S. M. Jones, M. D. Barber, L. J. Streletz, Topographic mapping of human motor cortex with transcranial magnetic stimulation: Homunculus revisited, Brain Topography (1993) 13–19. doi:https://doi.org/10.1007/BF01234122.

[21] M. Lacerenza, L. Spinelli, M. Buttafava, A. D. Mora, F. Zappa, A. Pifferi, A. Tosi, B. Cozzi, A. Torricelli, D. Contini, Monitoring the motor cortex hemodynamic response function in freely moving walking subjects: a time-domain fNIRS pilot study, Neurophotonics 8 (2021) 015006. URL: https://doi.org/10.1117/1.NPh.8.1.015006. doi:10.1117/1.NPh.8.1.015006.

[22] M. Shadaydeh, L. Müller, D. Schneider, M. Thümmel, T. Kessler, J. Denzler, Analyzing the direction of emotional influence in nonverbal dyadic communication: A facial-expression study, IEEE Access 9 (2021) 73780–73790. doi:10.1109/ACCESS.2021.3078195.

Appendix A: fNIRS data visual quality check using Wavelet transform

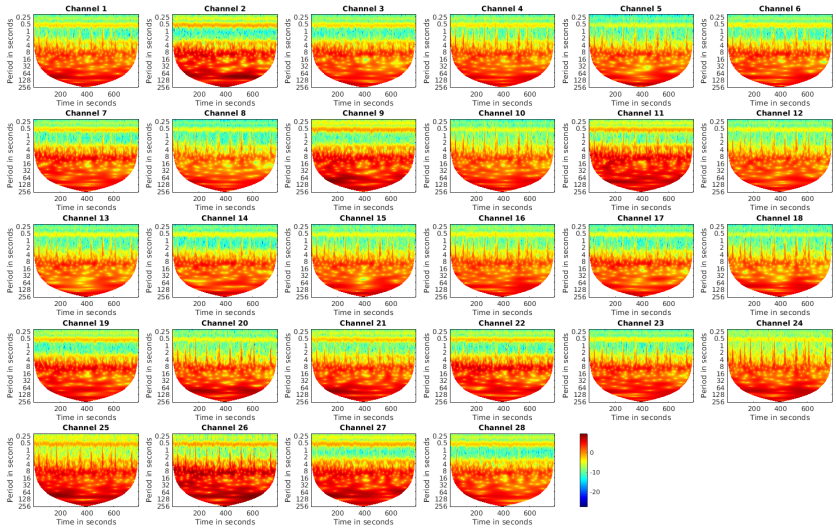

(a) Good quality data

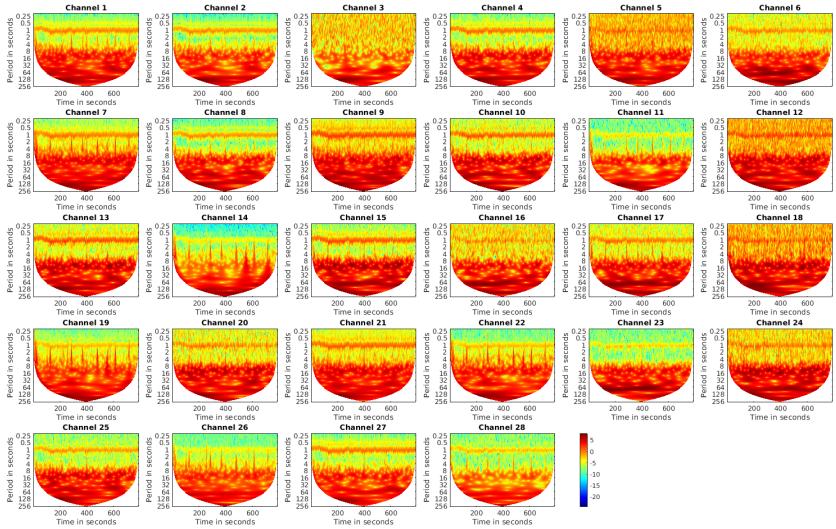

(b) Bad quality data

Figure 5: fNIRS data visual quality check using Wavelet transform plots before any filtering: (a) a good quality data with a clear separation between the heart rate at the period of $\approx 1sec$ and the lower frequencies (higher periods) and (b) a bad quality data where high wavelet values occur at all frequencies and all time samples.

Appendix B: True Positive Rate and F-score Plots

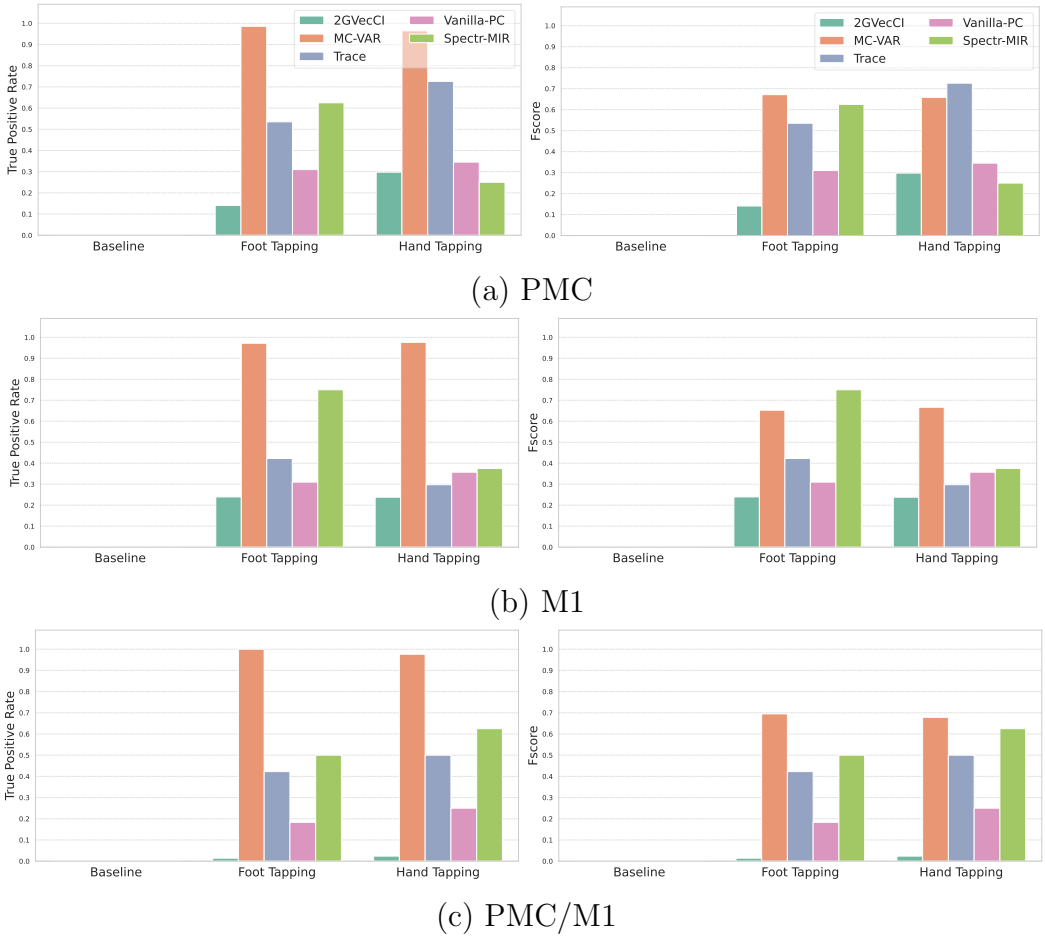

(a) PMC

(b) M1

(c) PMC/M1

Figure 6: The true positive rate (TPR) (left) and F1-score (right) of the time domain cause-effect analysis results for the normalized HbO time series using the Spectr-MIR method in comparison with four baseline methods: Vanilla-PC [11], 2GVecCI [10], Trace [9], and MC-VAR [12] for the three different regions: (a) Primary Motor Cortex (PMC), (b) Motor Cortex (M1), and (c) PMC/M1. MC-VAR shows high TPR and high FPR(Figure 4), indicating that this method detects causal links everywhere.